DALTON
FULL PAPER

A dynamical density functional study of CO insertion into the metal–alkyl bond in $Ti(Cp)_2(CH_3)_2$

Filippo De Angelis,[a] Antonio Sgamellotti *[a] and Nazzareno Re[b]

[a] *Dipartimento di Chimica e Centro di Studio CNR per il Calcolo Intensivo in Scienze Molecolari, Università di Perugia, I-06123 Perugia, Italy*
[b] *Facoltà di Farmacia, Università G. D'Annunzio, I-66100 Chieti, Italy*

Received 7th December 2000, Accepted 9th February 2001
First published as an Advance Article on the web 15th March 2001

The migratory insertion of CO into the titanium–methyl bond in $Ti(Cp)_2(CH_3)_2$ has been investigated by both static and dynamic density functional calculations. CO coordination prior to insertion has been analysed considering both "lateral" and "central" approaches, finding the two pathways kinetically equivalent. The relative stability of the O-outside and O-inside η^2-bound acyl complexes has been investigated, finding the O-outside isomer more stable by 4.0 kcal mol^{-1}, with an energy barrier for the conversion from the O-outside isomer of 9.6 kcal mol^{-1}. Dynamic simulations have also been performed on the $Ti(Cp)_2(CH_3)_2$–CO adduct in order to study the detailed features of the CO migratory insertion and of the η^1- $\longrightarrow$ η^2-acyl conversion, and show that migratory insertion takes place within 1 ps through detachment of the methyl group upon CO migration, leading to an O-inside η^2-acyl complex.

1 Introduction

There has been much interest in the migratory insertion of carbon monoxide into metal–alkyl and metal–hydride bonds.[1–9] Insertion in metal–alkyl bonds has been observed for most early d-block metals as well as for several actinide and lanthanide elements. In particular many studies have shown that Group 4 metallocene substrates of the type $M(Cp)_2(R)X$ (R = alkyl; X = alkyl, halide, alkoxide, *etc.*) easily react with CO to give the corresponding acyls complexes, eqn. (1) (M = Ti,

$$M(Cp)_2(R)X + CO \longrightarrow M(Cp)_2(\eta^2\text{-}RCO)X \qquad (1)$$

Zr or Hf). Spectroscopic data and structural studies have indicated that all these acyl complexes show an η^2-bonding mode where both carbon and oxygen atoms are bound to the metal

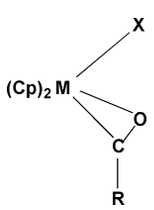

Scheme 1

(see Scheme 1). The unique reactivity of the coordinated acyls has been attributed to this η^2-bonding mode.

There are two possible isomers of these η^2-acyl complexes, one with the oxygen atom directed away from the additional ligand X and the other with the oxygen directed towards X. These are conventionally indicated as, respectively, "O-outside" and "O-inside" and are illustrated as **A** and **B** in Fig. 1. Structural characterization of isolable biscyclopentadienyl acyl complexes of Ti and Zr gave evidence only of the "O-inside" isomer, which is therefore the thermodynamically most stable form. However, detailed mechanistic studies on the carbonylation of $Zr(Cp)_2(CH_3)_2$ by Erker[7] have shown that the low temperature kinetically controlled CO insertion leads to the O-outside η^2-acyl isomer. This species isomerizes to the thermodynamically more stable O-inside isomer, only above

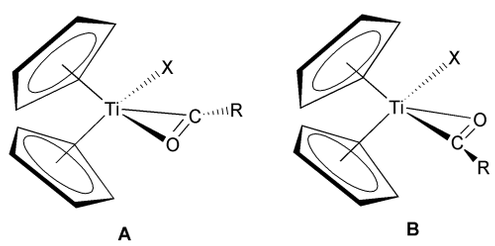

Fig. 1 Structure of the O-inside and O-outside η^2-acyl complexes.

−60 °C. These results were interpreted in terms of the CO molecule initially binding to the metal on the outside (**A**), rather than between the two alkyl groups (**B**), see Scheme 2. Although

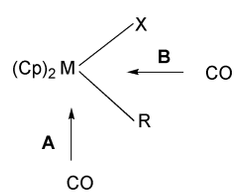

Scheme 2

the CO insertion into biscyclopentadienyl dialkyl titanium complexes has been suggested to follow the same pathway,[9] no mechanistic studies have been performed on this reaction to date.

Isolated η^2-acyl complexes are very reactive and undergo a variety of interesting transformations.[8,10] The most common reactions of mixed alkyl–acyl complexes are: (i) insertion of the alkyl group into the acyl moiety to generate a η^2-ketone; (ii) insertion of a second CO molecule to give an enediolate complex. These reactions will be the subject of a forthcoming paper.

Previous calculations at the extended Hückel level of theory have been performed on CO insertion in bis(cyclopentadienyl)metal dimethyl complexes.[9–11]

In a recent paper we have reported static density functional theory (DFT) calculations on migratory insertion of CO into the zirconium–methyl bond in $Zr(Cp)_2(CH_3)_2$.[12] In the present

report we study CO insertion into the titanium–methyl bond in $Ti(Cp)_2(CH_3)_2$ in order to point out analogies and differences with the corresponding zirconium complex. Moreover, we have combined 'static' DFT calculations on the stationary points of the potential surface with first principle molecular dynamics calculations based on the Car–Parrinello approach.[13] Static DFT calculations have been performed in order to compute the geometries and the relative stabilities of the stationary points of the potential energy surface for the CO insertion including all possible isomers of the resulting alkyl–acyl complex. Car–Parrinello simulations have been employed to study the hitherto inaccessible dynamic features of (i) the carbonyl migratory insertion from the $Ti(Cp)_2(CH_3)_2$–CO adduct to the acyl complex, (ii) the conversion of the O-outside η^1-acyl complex into the more stable η^2 form.

2 Computational details

Static DFT calculations

The static DFT calculations reported in this work have been performed using the GAUSSIAN 98 program package.[14] We used a 6-311G*,[15–17] basis set for the titanium, chlorine and oxygen atoms and for the carbon and hydrogen atoms in the CO and CH_3 groups, while a 6-31G*[18] basis set was employed for the carbon and hydrogen atoms in the cyclopentadienyl groups, for a total of 296 basis functions. The chosen basis set represents a very good trade off between accuracy and saving in computational power and was used to obtain thermochemical and kinetic data. Geometry optimizations were performed on all the stationary points of the potential energy surface for the CO insertion, considering the Vosko–Wilk–Nusair LDA (local density approximation) parameterization[19] and including the Becke[20] and Perdew–Wang[21] gradient corrections (GC) to the exchange and correlation, respectively. The transition states for the key steps of the migratory insertion have been determined using the synchronous transition-guided quasi-Newton method available in GAUSSIAN 98[22] and checked by frequency calculations.

Car–Parrinello calculations

Molecular dynamics simulations were carried out with the Car–Parrinello (CP) method.[13,23] The calculations reported here have been performed with the parallel version, developed by one of us (F.D.A.), of the CP code implementing Vanderbilt pseudopotentials.[23] For the LDA exchange-correlation functional the Perdew–Zunger parameterization[24] has been used, while the gradient-corrected functional is taken from ref. 25. Core states are projected out using pseudopotentials. For Ti, C and O "ultra-soft" pseudopotentials were generated according to the scheme proposed by Vanderbilt,[26] whereas for Cl the Bachelet–Hamann–Schlüter (BHS) pseudopotential[27] has been used. The wavefunctions were expanded in plane waves up to an energy cutoff of 25 Ry. Periodic boundary conditions were used by placing the model molecule in a cubic box of 10.6 Å, keeping a minimum of 5 Å between repeated images, sufficiently large to avoid coupling between periodic images. The equations of motion were integrated using a time step of 6 au (0.145 fs) with an electronic fictitious mass $\mu = 2000$ au.

In order to check the consistency of the CP and GAUSSIAN 98 programs, we compared the geometries of the fully optimized O-inside η^2-acyl chloride complex $Ti(Cp)_2(\eta^2\text{-}COCH_3)Cl$, for which experimental data are available.[28] In Table 1 optimized geometrical parameters computed with the CP and GAUSSIAN 98 programs have been reported and show a good agreement between the two approaches and experimental data. An interesting point is that both the CP and GAUSSIAN 98 approach led to almost the same value for the distance between the metal and the cyclopentadienyl carbons (average value), which suggests that metal–Cp interactions are accounted for with the same accuracy within both approaches.

Table 1 Optimized geometrical parameters (Å and degrees), computed with the CP and GAUSSIAN 98 programs, together with experimental data, for the O-inside $Ti(Cp)_2(\eta^2\text{-}COCH_3)Cl$ complex

Parameter	CP	G98	Exp.[28]
$r_{Ti-C=O}$	2.053	2.067	2.071
$r_{Ti-O=C}$	2.256	2.278	2.194
$r_{C=O}$	1.271	1.234	1.18
$r_{Ti-O} - r_{Ti-C}$	0.20	0.21	0.12
Ti–C=O	82.6	83.2	79.7

3 Results and discussion

Two different conformers of the dialkyl complex $Ti(Cp)_2(R)_2$, **1**, can be conceived, corresponding to an eclipsed and a staggered arrangement of the two cyclopentadienyl groups. Geometry optimizations performed on complex **1** led to an eclipsed arrangement of the two cyclopentadienyl groups, with the staggered conformer 0.6 kcal mol^{-1} higher in energy. For the most stable eclipsed arrangement the optimized CH_3–Ti bond distance was 2.181 Å with the CH_3–Ti–CH_3 angle computed to be 93.8°.

Hereafter we will consider only the eclipsed conformer as the starting geometry of all the structures analysed in this work, which allows one to exploit the computational savings due to the C_s symmetry.

3.1 CO coordination by the metal

Coordination of the electrophilic CO molecule at an electron deficient metal center has been proposed as the initial step of the migratory insertion reaction. Previous extended Hückel calculations[9] have indicated that the only vacant molecular orbital to which the incoming CO ligand can donate is of a_1 symmetry, essentially a hybrid d orbital directed along the *y* axis between the metallocene sandwich. According to this bonding picture the CO is expected to attack along the line perpendicular to the Cp centroid–metal–Cp centroid plane (**A**), rather than between the two methyl groups (**B**), see Scheme 2.

At variance with this picture, our accurate DFT calculations show an isolated LUMO of a_1 symmetry composed of two equivalent lobes pointing along the *y* and *z* axis. Therefore, in order to check which attack direction is the most favorable, we performed geometry optimizations on the final five-coordinated complexes resulting from lateral and central attacks and a transition state search for both pathways. In order to check whether out of plane pathways were energetically accessible, we performed transition state optimizations without any symmetry constraints.

(A) Lateral coordination. Geometry optimization performed on the lateral five-coordinated CO–$Ti(Cp)_2(CH_3)_2$ adduct, **2a** (see Fig. 2), led directly to an η^1-acyl complex. In order to evaluate the barrier for the lateral CO approach, we performed a linear transit scan of the potential energy surface of the system composed by $Ti(Cp)_2(CH_3)_2$ + CO assuming the carbonyl carbon–titanium distance as a reaction coordinate; constrained geometry optimizations were performed by keeping this parameter fixed at selected values in the range 2.0–4.0 Å, and by optimizing all the other parameters. The resulting curve shows a maximum for a value of the reaction coordinate of *ca.* 2.7 Å, 15.6 kcal mol^{-1} above the isolated reagents. We then performed a transition state optimization for lateral CO coordination starting from the maximum energy structure encountered during the linear transit, finding a structure 15.0 kcal mol^{-1} higher in energy than the free reagents, for a value of the

Table 2 Optimized geometrical parameters (Å and degrees), for the five-coordinated CO adducts **2b** and **2c** and for the transition state for the migratory insertion from **2b**

Parameter	**2b**	**2c**	**TS**
$r_{Ti-C=O}$	2.045	2.389	2.036
$r_{C=O}$	1.160	1.154	1.182
r_{Ti-C_α}	2.386	2.330	2.627
r_{Ti-C_β}	2.386	2.330	2.281
$r_{Ti-C_{Cp}}$ (Av.)	2.411	2.777	2.405
Ti–C=O	178.6	180.0	164.5
CH_3–Ti–CH_3	129.6	98.7	121.2

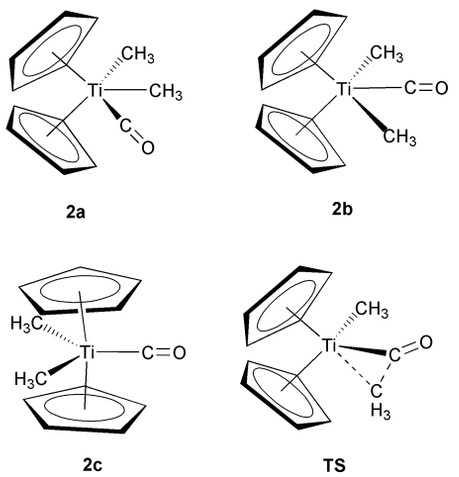

Fig. 2 Structures of the three considered CO five-coordinated adducts **2a**, **2b** and **2c** and of the transition state for the migratory insertion starting from **2b**.

carbon–titanium distance of 2.696 Å. Eigenvector analysis performed on the computed transition state revealed that the reaction coordinate is largely composed by the metal–CO distance, which therefore represents a good approximation to the computed reaction mode.

(B) Central coordination. Geometry optimization of the CO five-coordinated adduct resulting from central attack between the two CH_3 groups, **2b**, led to a structure almost isoenergetic (0.3 kcal mol^{-1} lower) with the free reagents. Frequency calculations performed on the optimized geometry showed that this structure is a true minimum on the potential energy surface. The resulting structure reveals an almost planar arrangement of the CO and CH_3 ligands (see Fig. 2 and Table 2), with the C, O and Ti atoms almost collinear (O–C–Ti 178.6°); the Ti–CH_3 distance was 2.386 Å, with a CH_3–Ti–CH_3 angle of 129.6°. The Ti–C(CO) distance was 2.045 Å, suggesting quite a weak interaction between the CO ligand and the $Ti(Cp)_2(CH_3)_2$ fragment, as expected since the CO ligand cannot exert any stabilizing π-back donation interaction with a d^0 electron deficient metal center such as Ti^{IV}.

For the sake of completeness we searched also for trigonal bipyramidal isomers, finding a very unstable structure, **2c**, with the two Cp ligands in axial positions, which we computed to be 42.1 kcal mol^{-1} higher in energy than the free reagents. The structures of the five-coordinated isomers are illustrated in Fig. 2, while a list of the main geometrical parameters can be found in Table 2.

In order to obtain the energy barrier to central coordination, we searched for the corresponding transition state, finding a barrier of 15.2 kcal mol^{-1}, with respect to the free reagents, for a value of the Ti–C distance of 2.912 Å. Eigenvector analyses performed on this transition state have shown almost negligible coefficients for all the internal geometrical coordinates except the Ti–CO distance.

Table 3 Optimized geometrical parameters (Å and degrees) for the O-inside η^2-acyl (**3**), O-outside η^2-acyl (**4a**) and η^1-acyl (**4b**) $Ti(Cp)_2(CO)(CH_3)_2$ complexes and for the transition state for the O-outside η^2-acyl ⟶ O-inside η^2-acyl conversion

Parameter	**3**	**4a**	**4b**	**TS**
$r_{Ti-C=O}$	2.075	2.090	2.232	2.338
$r_{Ti-C=C}$	2.287	2.248	3.157	3.120
$r_{C=O}$	1.239	1.243	1.221	1.223
$r_{Ti-O} - r_{Ti-C}$	0.212	0.158	0.925	0.782
Ti–C=O	83.2	80.5	129.8	120.0

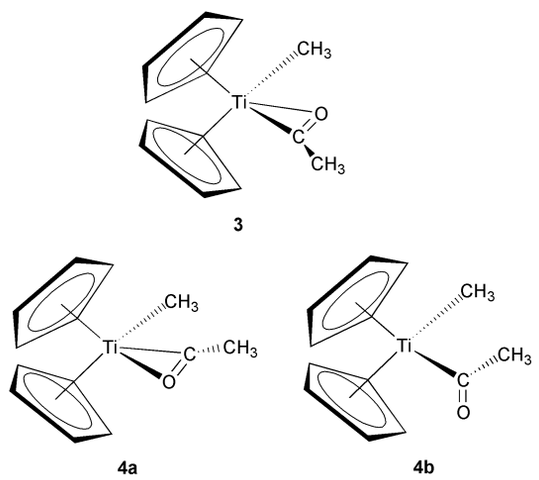

Fig. 3 Structures of the O-inside and O-outside η^2-acyl and O-outside η^1-acyl complexes **3**, **4a** and **4b**.

By comparing the results for the lateral and central attacks we see that the two processes show essentially isoenergetic barriers (15.0 and 15.2 kcal mol^{-1}, respectively) which suggests that both pathways should be kinetically equivalent. This behavior is different from that found for migratory insertion of CO into the Zr–CH_3 bond, for which the energy barrier for lateral attack is 5.0 kcal mol^{-1} lower.[12] Indeed, the O-outside acyl isomer is observed as a preliminary product of the insertion reaction of CO into the Zr–CH_3 bond,[8] while such a product has never been observed for the corresponding titanium system.

3.2 CO insertion and η^2-acyl complexes

We searched for the transition state for the migratory insertion reaction which properly correlates with the central CO adduct **2b**, finding a structure 2.8 kcal mol^{-1} higher in energy than the corresponding reagent, and, therefore 2.5 kcal mol^{-1} above the energy of the free reagents. The geometry of this transition state was found quite similar to that of the corresponding five-coordinated adduct, with the carbonyl group slightly bent towards the inserting alkyl group and an O-inside arrangement of the acyl group, see Fig. 2 and Table 2.

We optimized the geometry of the O-inside η^2-acyl complex, **3**, finding it 19.7 kcal mol^{-1} below the reagents while no O-inside η^1-acyl minimum was found on the potential energy surface; we can therefore deduce that the migratory insertion reaction starting from **2b** should lead directly to the η^2-acyl complex **3**. The structure of **3** has been plotted in Fig. 3, while a list of the main optimized geometrical parameters can be found in Table 3.

As discussed above, any attempt to optimize the lateral five-coordinated $Ti(Cp)_2(CH_3)_2$–CO adduct led directly to the O-outside η^1-acyl complex, **4b**, so that there should be no transition state for the migratory insertion reaction correlated with lateral CO attack. We also optimized the geometry of the O-outside η^2-acyl complex, **4a**, finding a structure 4.0

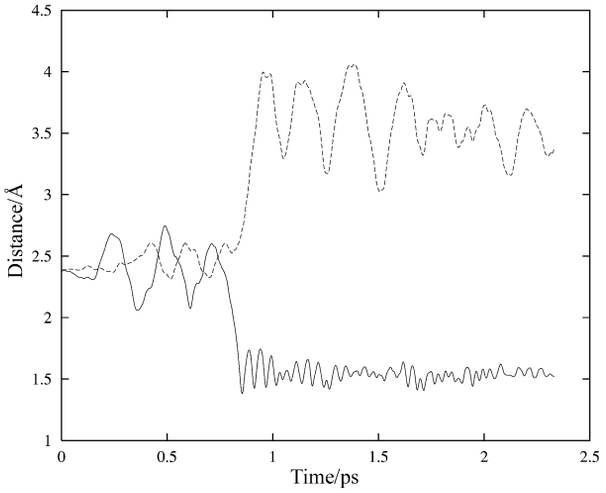

Fig. 4 Time evolution of the C_α–C (inserting CH_3–CO), solid line, and C_α–Ti, dashed line, distances for the dynamics simulation starting from the central five-coordinated CO adduct **2b**.

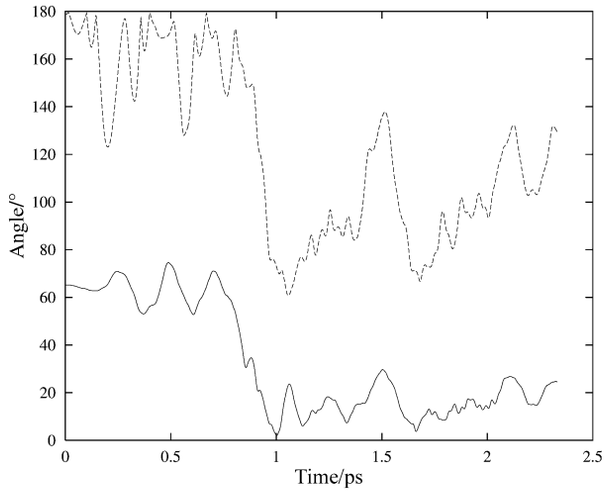

Fig. 5 Time evolution of the C_α–Ti–C (inserting CH_3–CO), solid line, and of the O–C–Ti (carbonyl), dashed line, angles for the dynamics simulation starting from the central five-coordinated CO adduct **2b**.

kcal mol^{-1} above the O-inside isomer **3**, in agreement with experimental evidence; indeed, all X-ray analyses of isolated $M(Cp)_2(X)(COR)$ acyl complexes revealed an O-inside η^2 coordination.

3.3 O-Outside η^1-acyl ⟶ η^2-acyl conversion

The O-outside η^1-acyl minimum, **4b**, is 3.9 kcal mol^{-1} higher in energy than the corresponding η^2-bound isomer. Structures of **4a** and **4b** can be found in Fig. 3, while a list of the main optimized geometrical parameters is in Table 3. We checked the presence of an activation barrier for the O-outside η^1- ⟶ η^2-acyl conversion, by performing a linear transit scan of the potential energy surface for the O-outside complexes. The O–C–Ti angle was constrained at selected values in the range 80–140°, fully relaxing all the other geometrical parameters, expecting this approximate reaction coordinate to connect smoothly the two isomers. The calculated potential energy curve shows a very small barrier (*ca.* 1 kcal mol^{-1}), for a value of the O–C–Ti angle of about 110°. We finally optimized the geometry of the transition state for the η^1 ⟶ η^2 conversion, finding an activation barrier of only 0.6 kcal mol^{-1}.

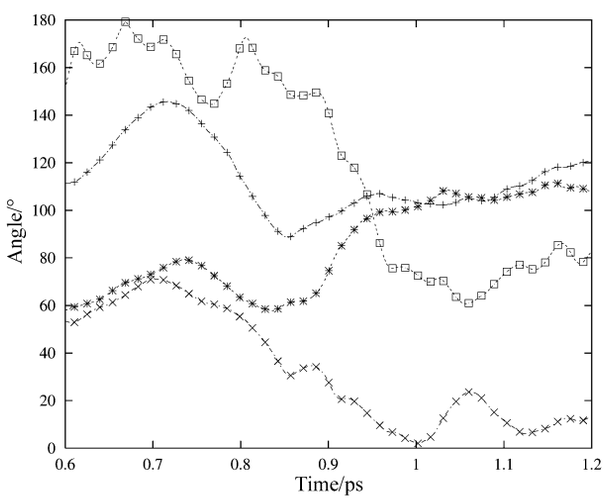

Fig. 6 Time evolution of the O–C–Ti (□), C_α–Ti–C_β (+), C_β–Ti–C (∗) and C_α–Ti–C (×) angles during the time span from 0.6 to 1.2 ps for the dynamics simulation starting from the central five-coordinated CO adduct **2b**.

3.4 Dynamics calculations

3.4.1 Central CO insertion. We started the dynamics simulation of the migratory insertion reaction by heating up the structure of the five-coordinated CO adduct **2b** in the geometry obtained by the static DFT optimization, at a temperature of 300 K. To obtain a thermal distribution of vibrational modes the temperature was gradually increased (*via* rescaling of ionic velocities) by small steps. Owing to the low energy barrier, we did not apply any constraints to the molecular motion, allowing all the degrees of freedom to evolve naturally in time. The time span of the simulation was 2.5 ps.

The evolution of the CO migratory insertion can be followed by studying the time evolution of several geometrical parameters, such as the CO–CH_3 carbon–carbon distance and the CH_3 carbon–titanium distance. Indeed, the CO–CH_3 carbon–carbon distance is *ca.* 2.4 Å in reagent **2b**, where the two carbon atoms belong to two different ligands, while it is only *ca.* 1.5 Å in the acyl product, where they are directly bound. The CH_3 carbon–titanium distance is *ca.* 2.4 Å in the reagent while it grows to *ca.* 3.5 Å in the product where the CH_3 group and the metal are no longer bound. Fig. 4 displays the variation of the CO–CH_3 carbon–carbon distance and of the CH_3 carbon–titanium distances as a function of the simulation time. It appears that the reactive CO migration takes place within *ca.* 1 ps. Indeed, a fast decrease in the C–C distance from *ca.* 2.4 to *ca.* 1.5 Å is observed around 0.8 ps. Thereafter, the C–C distance varies within the normal limits of C–C vibration. Moreover, we notice how the CH_3 carbon–titanium distance follows almost a complementary trajectory with respect to the C–C distance; nevertheless this parameter shows higher oscillations, after 1 ps, due to the fact that, at the end of the reaction, the Ti and C atoms are no longer bound. The achievement of the CO migration is confirmed by the time evolution of the C–Ti–C angle (CH_3 and CO carbons) plotted in Fig. 5, which decreases from *ca.* 65°, close to its equilibrium value in **2b**, to *ca.* 20° reflecting the approach of the carbonyl to the methyl group.

In order to rationalize whether a possible O-inside η^1-acyl structure plays some role as a reaction intermediate, we have analyzed the evolution of the O–C–Ti angle as a function of the simulation time. Indeed, the chosen parameter characterizes both the CO adduct **2b** and the acyl complexes, decreasing from *ca.* 180 to *ca.* 130 to *ca.* 80°, on going from the adduct **2b** to an eventual η^1-acyl to the η^2-acyl complex, respectively. The O–C–Ti angle has been plotted as a function of the simulation time in Fig. 5. It is evident that the CO migratory insertion leads directly to the η^2-acyl complex; indeed, a fast decrease in the O–C–Ti angle from its value in the five-coordinated isomer **2b** to that characteristic of the η^2-acyl complex is observed

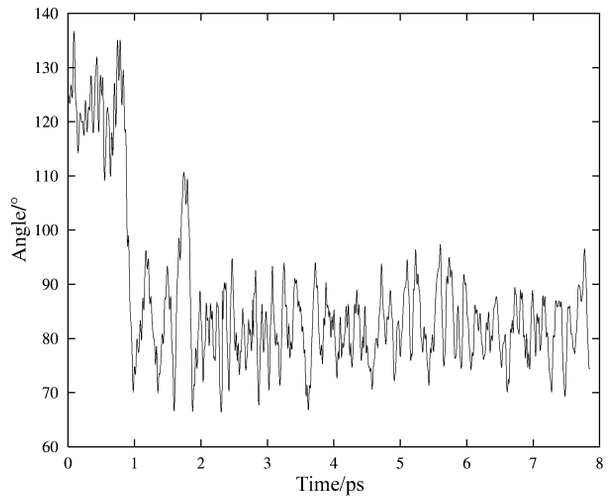

Fig. 7 Time evolution of the O–C–Ti (carbonyl) angle during the dynamics simulation starting from the O-outside η^1-acyl complex **4b**.

within 1 ps in correspondence to CO migration. Thereafter the considered angle oscillates between the values characteristic of the η^2- and η^1-acyl complexes.

In order to describe the reaction mechanism of the migratory insertion in more detail, we have analyzed the time evolution of the O–C–Ti, C_α–Ti–C_β (C_α is the carbon of the inserting methyl, C_β that of the non-inserting methyl and C is the carbonyl carbon), C_β–Ti–C and C–Ti–C_α angles, for the time span from 0.6 to 1.2 ps, which includes the beginning of the insertion reaction at *ca*. 0.7 ps. The results, collected in Fig. 6, show a decrease in C_α–Ti–C_β starting at *ca.* 0.7 ps, leading to a minimum at *ca.* 0.9 ps. At the same time both the C_β–Ti–C and the C_α–Ti–C angles show a similar decrease, accompanied by an out of plane oscillation of the O–C–Ti angle which decreases to *ca.* 140°. This means that the two methyls "squeeze" the CO group in the middle of a bending of the C_α–Ti–C_β angle, such that the bent CO group is ready to attack one of the methyl groups. This picture is consistent with the structure computed for the transition state for the insertion reaction from **2b**, which shows a reduced value of the C_α–Ti–C_β angle with respect to **2b** (121.2 *vs.* 129.6) and the CO group bent towards the inserting methyl, see Fig. 2. From the previous discussion we can conclude that CO insertion occurs *via* a simultaneous detachment of the methyl from the metal and formation of the carbon–carbon bond upon CO migration, leading directly to the O-inside η^2-acyl complex.

3.4.2 O-Outside η^1- ⟶ η^2-acyl conversion. In order to investigate the $\eta^1 \longrightarrow \eta^2$ conversion we performed molecular dynamics simulations by heating up the structure of the stable O-outside η^1-acyl complex **4b**, in the geometry optimized by our static DFT calculations. The system was thermalized at 300 K by gradually increasing the temperature in small steps; the time span of the simulation was 7.8 ps. As discussed above, the formation of the O-outside η^2-acyl complex might be rationalized by investigating the time evolution of the O–C–Ti angle, which has been plotted in Fig. 7. As can be noticed, the conversion between the two O-outside acyl complexes takes place within 1 ps. Indeed, a fast decrease of the angle from its value in the η^1-acyl (*ca.* 120°) to that characteristic of the η^2-acyl complex (*ca.* 80°) is observed starting at *ca.* 0.8 ps. After 1 ps the O–Ti–C angle oscillates around its equilibrium value for the η^2-acyl complex. We extended the time span of the simulation up to *ca.* 8 ps in order to check the presence of an η^1- ⟶ η^2-acyl equilibrium, analogous to that partially observed for the O-inside η^2-acyl complex. In the O-outside case, however, no such equilibrium seems to exist at the considered temperature.

3.5 O-Outside ⟶ O-inside conversion

The transition state for the O-outside η^2-acyl ⟶ O-inside η^2-acyl conversion has been optimized, finding a η^1 structure with an O–C–Ti–C dihedral angle of 83.2°. Frequency calculations revealed that the computed structure is a true transition state (one imaginary frequency) with the reaction coordinate largely composed by the O–C–Ti–C dihedral angle. Selected geometrical parameters for this transition state have been reported in Table 3; the computed structure reveals an η^1 arrangement of the acyl ligand, as suggested by the longer Ti–OC distance (3.120 Å) and by the value of the Ti–C–O angle, 120.0°. Thus, the conversion between the two η^2-acyl isomers seems to involve the loss of η^2 coordination. This transition state was found 9.6 kcal mol^{-1} higher in energy than the O-outside η^2-acyl complex, 2.6 kcal mol^{-1} lower than for the corresponding $Zr(Cp)_2(CH_3)(COCH_3)$ systems. Although no experimental data are available for the O-outside η^2-acyl ⟶ O-inside η^2-acyl interconversion in bis(cyclopentadienyl)-titanium complexes, NMR studies of non-cyclopentadienyl Group 4 metal complexes such as $M(OAr)_2(\eta^2\text{-}RCNR')_2$ iminoacyl complexes[29] have shown that the energy barrier for the titanium complex is 1.1 kcal mol^{-1} lower than in the zirconium complex, thus supporting our calculations. Owing to the relatively high energy barrier obtained by the above transition state calculation we did not perform molecular dynamics simulation on the conversion between the two η^2-acyl isomers.

3.6 Energetics of the migratory insertion

From all the above calculations we can now build the energy profile for the overall migratory insertion reaction, by combining the energies of the intermediates and transition states for all the considered steps. A schematic representation of the potential energy surface for the overall reaction, obtained considering the minimum energy structures for intermediates and transition states, has been plotted in Fig. 8. As can be noticed, all the steps involved in the migratory insertion after CO coordination are exothermic and the final thermodynamically most stable O-inside η^2-acyl product lies 19.7 kcal mol^{-1} below the reagents. We computed the energy barriers for CO coordination to be 15.0 and 15.2 kcal mol^{-1} for lateral and central attacks, while lower (2.8 kcal mol^{-1}) or negligible energy barriers (0.6 kcal mol^{-1}) were found for the migratory CO insertion reaction and for the O-outside $\eta^1 \longrightarrow \eta^2$ conversion, respectively, so that the barrier to CO coordination (*ca.* 15 kcal mol^{-1}) represents the overall energy barrier for the migratory insertion reaction. We computed the barrier for the O-outside η^2-acyl ⟶ O-inside η^2-acyl conversion to be 9.6 kcal mol^{-1}, still 5.8 kcal mol^{-1} lower than the energy of the free reagents and 2.6 kcal mol^{-1} lower than the energy barrier computed for the O-outside η^2-acyl ⟶ η^2-acyl O-inside conversion in the corresponding zirconium complex, in agreement with the experimental trend.

4 Conclusion

The migratory insertion reaction of CO into the titanium–alkyl bond in $Ti(Cp)_2(CH_3)_2$ has been investigated by means of both static and dynamic density functional calculations. CO coordination processes prior to insertion have been analyzed considering both the case of lateral and central coordination to the metal leading, respectively, to formation of the O-outside and O-inside η^2-bound acyl complexes. We found the two CO coordination modes to be kinetically equivalent, a different behavior from that for migratory insertion of CO into the $Zr–CH_3$ bond for which the O-outside η^2-acyl isomer is observed as preliminary product. We optimized the geometries of the two possible η^2-bound acyl complexes, corresponding to the O-inside and O-outside isomers, finding the former to be

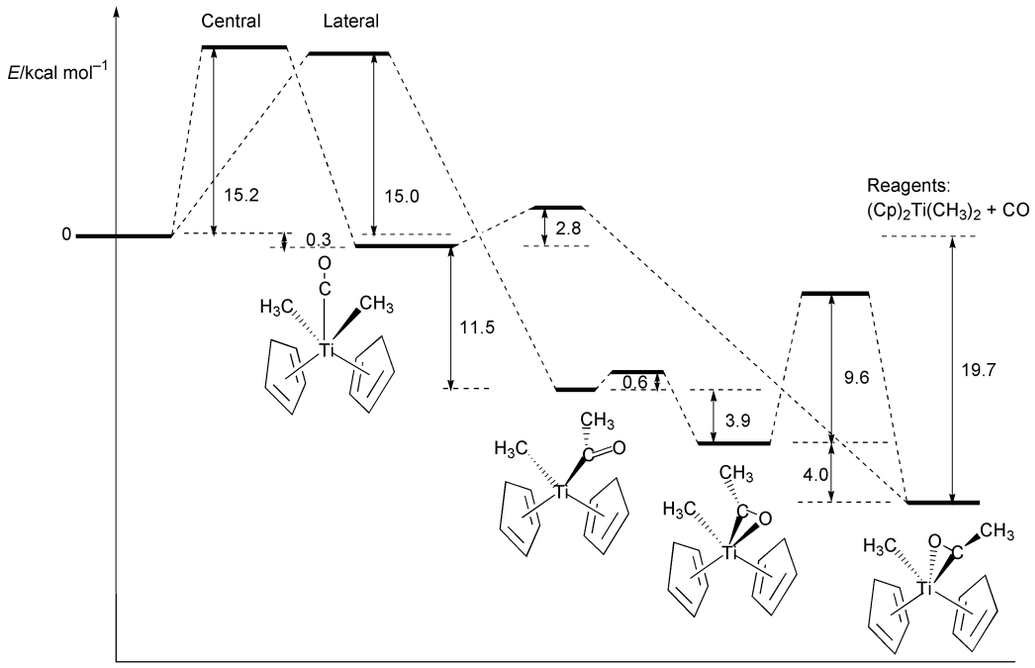

Fig. 8 Schematic representation of the potential energy surface for migratory CO insertion.

more stable by 4.0 kcal mol^{-1} again in agreement with the observed experimental trend.

We computed an energy barrier for the conversion between the two η^2-acyl isomers of 9.6 kcal mol^{-1}, 2.6 kcal mol^{-1} lower than that for the corresponding zirconium complex, a result which is supported by ^{1}H NMR experimental data on analogous non-cyclopentadienyl Group 4 complexes.[29]

Dynamic simulations performed on the central five-coordinated CO adduct have shown that the migratory insertion of CO into the titanium–methyl bond takes place within 1 ps by simultaneous detachment of the methyl and CO groups, leading directly to the O-inside η^2-acyl complex.

On the basis of thermodynamic and kinetic data we conclude that the migratory insertion reaction is a thermodynamically favored and kinetically easy process; the preliminary CO coordination was found to be the limiting step of the overall reaction.

Acknowledgements

We acknowledge CNR (Progetto Finalizzato "Materiali Speciali per Tecnologie Avanzate II") and MURST for financial support.

References

1 F. Calderazzo, *Angew. Chem., Int. Ed. Engl.*, 1977, **16**, 299.
2 E. J. Kulhmann and J. J. Alexander, *Coord. Chem. Rev.*, 1980, **33**, 195.
3 A. Wojcicki, *Adv. Organomet. Chem.*, 1973, **11**, 97.
4 T. C. Foold, *Top. Stereochem.*, 1981, **12**, 83.
5 J. J. Alexander, in *The Chemistry of the Metal–Carbon Bond*, ed. F. R. Hartley, Wiley, New York, 1985, vol. 2.
6 P. L. Bock, D. J. Boschetto, J. R. Rasmussen, J. P. Deneres and G. M. Whitesides, *J. Am. Chem. Soc.*, 1974, **96**, 2814.
7 G. Erker, *Acc. Chem. Res.*, 1984, **17**, 103.
8 L. D. Durfee and I. P. Rothwell, *Chem. Rev.*, 1988, **88**, 1059.
9 K. Tatsumi, A. Nakamura, P. Hofmann, P. Stauffert and R. Hoffmann, *J. Am. Chem. Soc.*, 1985, **107**, 4440.
10 P. Hofmann, P. Stauffert, M. Frede and K. Tatsumi, *Chem. Ber.*, 1989, **122**, 1559.
11 P. Hofmann, P. Stauffert, K. Tatsumi, A. Nakamura and R. Hoffmann, *Organometallics*, 1985, **4**, 404.
12 F. De Angelis, N. Re and A. Sgamellotti, *Organometallics*, 2000, **23**, 4904.
13 R. Car and M. Parrinello, *Phys. Rev. Lett.*, 1985, **55**, 2471.
14 GAUSSIAN 98 (Revision A.7), M. J. Frisch, G. W. Trucks, H. B. Schlegel, G. E. Scuseria, M. A. Robb, J. R. Cheeseman, V. G. Zakrzewski, J. A. Montgomery, R. E. Stratmann, J. C. Burant, S. Dapprich, J. M. Millam, A. D. Daniels, K. N. Kudin, M. C. Strain, O. Farkas, J. Tomasi, V. Barone, M. Cossi, R. Cammi, B. Mennucci, C. Pomelli, C. Adamo, S. Clifford, J. Ochterski, G. A. Petersson, P. Y. Ayala, Q. Cui, K. Morokuma, D. K. Malick, A. D. Rabuck, K. Raghavachari, J. B. Foresman, J. Cioslowski, J. V. Ortiz, B. B. Stefanov, G. Liu, A. Liashenko, P. Piskorz, I. Komaromi, R. Gomperts, R. L. Martin, D. J. Fox, T. Keith, M. A. Al-Laham, C. Y. Peng, A. Nanayakkara, C. Gonzalez, M. Challacombe, P. M. W. Gill, B. G. Johnson, W. Chen, M. W. Wong, J. L. Andres, M. Head-Gordon, E. S. Replogle and J. A. Pople, Gaussian, Inc., Pittsburgh, PA, 1998.
15 P. J. Hay, *J. Chem. Phys.*, 1977, **77**, 4377.
16 A. J. H. Wachters, *J. Chem. Phys.*, 1970, **52**, 1033.
17 M. J. Frisch, J. A. Pople and J. S. Binkley, *J. Chem. Phys.*, 1984, **80**, 3265 and references therein.
18 R. Ditchfield, W. J. Hehre and J. A. Pople, *J. Comput. Chem.*, 1971, **54**, 724.
19 S. H. Vosko, L. Wilk and M. Nusair, *Can. J. Phys.*, 1980, **58**, 1200.
20 A. D. Becke, *Phys. Rev. A*, 1988, **38**, 3098.
21 J. P. Perdew and Y. Wang, *Phys. Rev. B*, 1992, **45**, 13244.
22 J. Simons, P. Jorgensen, H. Taylor and J. Ozment, *J. Phys. Chem.*, 1983, **87**, 2745.
23 The implementation that we use is described in: A. Pasquarello, K. Laasonen, R. Car, C. Lee and D. Vanderbilt, *Phys. Rev. Lett.*, 1992, **69**, 1982; A. Pasquarello, K. Laasonen, R. Car, C. Lee and D. Vanderbilt, *Phys. Rev. B*, 1993, **47**, 10142.
24 J. P. Perdew and A. Zunger, *Phys. Rev. B*, 1981, **23**, 5048.
25 J. P. Perdew, J. A. Chevary, S. H. Vosko, K. A. Jackson, M. R. Pederson, D. J. Singh and C. Fiolhais, *Phys. Rev. B*, 1992, **46**, 6671.
26 D. Vanderbilt, *Phys. Rev. B*, 1990, **41**, 7892.
27 G. B. Bachelet, D. R. Hamann and M. Schlüter, *Phys. Rev. B*, 1982, **26**, 4199.
28 G. Facchinetti, C. Floriani and H. J. Stoeckli-Evans, *J. Chem. Soc., Chem. Commun.*, 1976, 522.
29 L. R. Chamberlain, L. D. Durfee, P. E. Fanwick, L. Kobriger, S. L. Latesky, A. K. McMullen, I. P. Rothwell, K. Folting, J. C. Huffman, W. E. Streib and R. Wang, *J. Am. Chem. Soc.*, 1987, **109**, 390.